Astron. Astrophys. 317, 898–906 (1997)

ASTRONOMY
AND
ASTROPHYSICS

Structure of L 1521B: CO observations of a dense core in Taurus

M. Juvela[1], **K. Lehtinen**[1], **K. Mattila**[1], **D. Lemke**[2], **and L. Haikala**[1]

[1]Helsinki University Observatory, Tähtitorninmäki, P.O.Box 14, SF-00014 University of Helsinki, Finland
[2]Max-Planck-Institut für Astronomie, Königstuhl 17, D-69117 Heidelberg, Germany

Received 17 February 1996 / Accepted 31 May 1996

Abstract. L 1521B is a dense core near B216 in one of the long filaments of the Taurus molecular cloud complex. The core is not associated with any known IR sources and shows no apparent signs of star formation. We have mapped the cloud in ^{13}CO(1–0) and C^{18}O(1–0) using a grid of 1′. This area, altogether some 140 square arc minutes, contains the density maximum as well as some parts of the filament north-west of the cloud centre. At the centre position we derive a column density N(C^{18}O)=4·10^{15}cm^{-2} and an optical depth of about 1.3 for C^{18}O. Using a value of r=140 pc for the distance we estimate that the total mass contained within a radius of 3′ around the density maximum is about 20 solar masses. The visual extinction has been estimated from the C^{18}O column density and through star counts of two fields observed at 2.2μm. The extinction in the central region is $A_V \approx 20^m$.

We have also mapped part of the B216 filament about one degree north-west of the centre of L 1521B in C^{18}O(1–0). This area contains two IRAS point sources which are probably associated with class I protostars.

Key words: ISM: clouds – ISM: molecules – ISM: L 1521B – radio lines: ISM

1. Introduction

L 1521B is a molecular core of large optical extinction in the long filamentary structure near B216 in the Taurus molecular cloud complex. The diameter of the opaque region on the red plates of the Palomar Sky Survey is about 7′ and the total area of visible extinction is 10′ × 150′ as determined by Myers et al. (1983). L 1521B has no associated IRAS sources.

The cloud was first identified as a high density core by Myers et al. (1979) who measured HC_5N(9-8) emission in the centre position ($04^h21^m08.5^s$+26°30′00″(1950.0)). Myers et al. (1983) also carried out measurements of ^{13}CO(1–0) and C^{18}O(1–0) at the centre position, where they found T_A^*(^{13}CO)=3.9 K and T_A^*(C^{18}O)=2.7 K. Based on these results they estimated an optical depth of τ(C^{18}O) = 1.2 and a column density N(C^{18}O) = 3.0· 10^{15} cm^{-2}. In their sample of 27 cores in the Taurus complex these values of τ(C^{18}O) and N(C^{18}O) were the second largest (after TMC–1). The value of the visual extinction derived from N(C^{18}O) exceeded 20^m.

Gaida et al. (1984) have performed star counts of the Taurus cloud complex using the Palomar Sky Atlas and a grid size of 4.5′ × 4.5′. For L 1521B they found only one field having A_V greater than 4.0^m and estimated a maximum extiction of 6.5^m. Using these values Gaida et al. estimated a mass of 33 $M_\odot$ for the field containing the extinction maximum. Myers et al. (1983) had calculated an upper limit 35 $M_\odot$ for the mass in a region of diameter 0.29 pc (7′at the distance of 140 pc). The filament containing L 1521B has a visual extinction $A_V > 2.5^m$ both to north-west and south-east of the centre. Cernicharo et al. (1985) have also carried out star counts on the Palomar Sky Atlas with a grid size of about 2.5′ finding visual extinctions comparable to those of Gaida et al.

In addition to the above mentioned detections of HC_5N(9-8), C^{18}O(1–0), ^{13}CO(1–0) and C^{12}O(1–0) there exist several other molecular line observations of the centre position of L 1521B. These include NH_3(1,1) (Benson & Myers 1989), HC_3N(4-3) (Sorochenko et al. 1986), HC_7N (Cernicharo et al. 1986) and C_3H_2 (Cox et al. 1989). Based on their measurements of C_3H_2 Cox et al. derived a central density of n(H_2) = 6.3·10^4 cm^{-3}. Sorochenko et al. (1986) estimated a density of 2·10^4 cm^{-3} which is the same as the upper limit 2·10^4 cm^{-3} given by Myers et al. (1983).

About one degree north-west of L 1521B there are two IRAS point sources (04181+2655 and 04181+2654) that indicate that ongoing star formation exists elsewhere in the filament (see e.g. Kenyon et al. 1990). At 2 μm the IRAS sources can be resolved into three separate components (Tamura et al. 1991), 04181+2654A, 04181+2654B and 04181+2655. The spectral energy distributions of all three sources correspond to class I protostars. One of these, 04181+2655, has been observed previously in CO(3–2) (Moriarty-Schieven et al. 1992) with some indication of high-velocity CO emission. Kenyon et al. (1993) have modelled the emission of the sources at infrared wavelengths using the solution for collapsing protostellar clouds by Terebey et al. (1984).

Send offprint requests to: M. Juvela

Table 1. Gaussian fit parameters for selected ^{13}CO(1–0) and C^{18}O(1–0) spectra in L 1521B. Column (1) gives the offsets in arc minutes from the centre position $04^h21^m08.5^s$+26°30′00″(1950.0). The gaussian line parameters are given in columns (2)–(4) and the error estimates given by the fitting routine are in parentheses. The line area in the last column is calculated directly as a sum of the channel values and is not a result of the fitting procedure

line & offset (′)	V (km s^{-1})	FWHM (km s^{-1})	T_A^* (K)	A (K km s^{-1})
^{13}CO(1–0)				
(2.3,-3.0)	6.62 (0.02)	1.66 (0.05)	3.5 (0.1)	6.4 (0.2)
(1.3,-3.0)	6.60 (0.02)	1.69 (0.06)	3.7 (0.2)	6.8 (0.2)
(0.0,-3.0)	6.66 (0.03)	1.88 (0.07)	3.0 (0.1)	6.1 (0.2)
(-1.0,-3.0)	6.59 (0.03)	1.91 (0.07)	3.4 (0.2)	6.9 (0.2)
(-2.3,-3.0)	6.57 (0.03)	1.91 (0.06)	3.5 (0.2)	7.1 (0.2)
(-3.3,-3.0)	6.64 (0.04)	1.72 (0.08)	3.2 (0.2)	5.4 (0.2)
(1.0, 1.0)	6.58 (0.02)	1.46 (0.04)	3.8 (0.2)	6.0 (0.2)
(1.0, 0.0)	6.67 (0.02)	1.49 (0.04)	3.7 (0.1)	6.2 (0.1)
(1.0,-1.0)	6.71 (0.02)	1.48 (0.04)	3.9 (0.1)	6.1 (0.1)
(0.0, 1.0)	6.59 (0.02)	1.51 (0.05)	3.7 (0.2)	6.0 (0.2)
(0.0, 0.0)	6.63 (0.01)	1.36 (0.04)	4.0 (0.1)	5.9 (0.1)
(-1.0,-1.0)	6.68 (0.02)	1.67 (0.04)	4.0 (0.1)	7.1 (0.1)
(-1.0, 1.0)	6.59 (0.01)	1.35 (0.04)	4.0 (0.1)	6.1 (0.1)
(-1.0, 0.0)	6.65 (0.01)	1.38 (0.03)	4.5 (0.1)	6.7 (0.1)
(-1.0,-1.0)	6.68 (0.02)	1.67 (0.04)	4.0 (0.1)	7.1 (0.1)
(-1.0,-2.0)	6.60 (0.02)	1.73 (0.06)	4.1 (0.2)	7.6 (0.2)
(-2.3,-1.0)	6.64 (0.02)	1.67 (0.05)	4.1 (0.2)	7.5 (0.2)
(-2.3,-2.0)	6.62 (0.03)	1.71 (0.07)	4.1 (0.2)	7.3 (0.3)
(-3.3,-1.0)	6.55 (0.03)	1.82 (0.07)	3.8 (0.2)	7.6 (0.2)
(-3.3,-2.0)	6.66 (0.02)	1.82 (0.06)	3.7 (0.2)	7.3 (0.2)
(3.5, 3.0)	6.55 (0.04)	1.85 (0.10)	3.3 (0.2)	6.8 (0.3)
(1.3, 3.0)	6.48 (0.03)	1.73 (0.08)	3.0 (0.2)	5.7 (0.2)
(-10.0,11.0)	6.56 (0.03)	1.37 (0.07)	3.1 (0.2)	4.0 (0.2)
(-9.0,10.0)	6.55 (0.03)	1.39 (0.08)	2.9 (0.2)	4.5 (0.2)
(-12.2,11.0)	6.67 (0.03)	1.35 (0.07)	3.3 (0.2)	5.5 (0.2)
(-11.2,10.0)	6.62 (0.03)	1.24 (0.08)	3.0 (0.3)	4.3 (0.2)
(-14.5,11.0)	6.54 (0.03)	1.21 (0.08)	3.0 (0.3)	4.5 (0.2)
(-13.5,10.0)	6.59 (0.02)	1.21 (0.04)	3.2 (0.2)	4.0 (0.1)
C^{18}O(1–0)				
(1.0, 1.0)	6.58 (0.03)	1.08 (0.07)	2.5 (0.2)	3.0 (0.2)
(1.0, 0.0)	6.42 (0.04)	0.86 (0.10)	2.4 (0.3)	2.6 (0.2)
(1.0,-1.0)	6.53 (0.04)	1.41 (0.11)	2.7 (0.3)	4.3 (0.3)
(0.0, 1.0)	6.53 (0.03)	0.99 (0.08)	3.3 (0.4)	3.2 (0.3)
(0.0, 0.0)	6.55 (0.02)	1.03 (0.06)	2.9 (0.2)	3.3 (0.2)
(0.0,-1.0)	6.73 (0.04)	1.22 (0.15)	3.0 (0.5)	5.3 (0.3)
(-1.0, 1.0)	6.58 (0.05)	1.1 (0.2)	2.1 (0.4)	3.2 (0.3)
(-1.0, 0.0)	6.58 (0.03)	0.98 (0.06)	2.6 (0.2)	2.5 (0.2)
(-1.0,-1.0)	6.73 (0.06)	1.2 (0.2)	2.7 (0.5)	4.6 (0.4)

The region around B216 has been part of some large scale mappings in ^{13}CO(1–0) (Kleiner & Dickman 1984, Heyer et al. 1987, Fukui and Mizuno 1991) and ^{12}CO(1–0) (Ungerechts & Thaddeus 1987). According to these, there exists a general velocity gradient along the filament with velocities increasing towards south-east, although this is not clear at the smaller scales of 10′ (Heyer et al. 1987). The area has been mapped previously also in ^{13}CO(1–0) and C^{18}O(1–0) by Duvert et al. (1986) who used a spacing of 5′ for their observations.

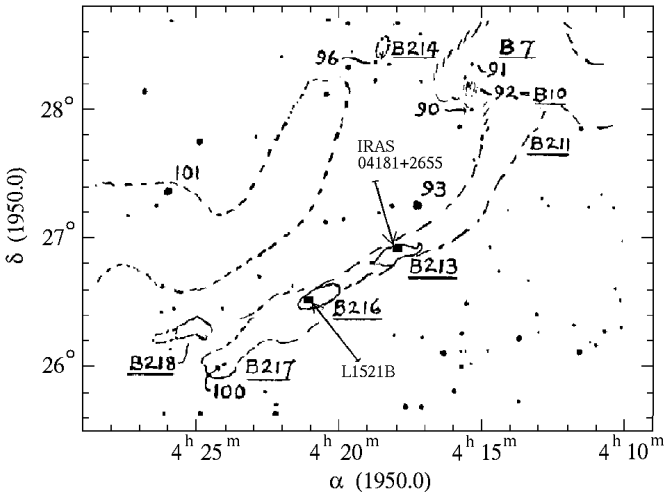

Fig. 1. The region around the cloud L 1521B in the Taurus molecular cloud complex according to Barnard (1927). The positions of mapped regions in L 1521B and around IRAS 04181+2655 are marked in the figure

The direction of the magnetic field around L 1521B is well determined from optical and near-IR polarization measurements (Moneti et al. 1984, Heyer et al. 1987, Goodman et al. 1992) and is perpendicular to the filament. The line of sight component of the magnetic field is comparably weak, though, and according to Zeeman measurements by Crutcher et al. (1993) is likely to be below 8 μG. It is still unclear, what role the magnetic field has in the dynamical development of L 1521B and the filament in general.

For the present study our motivation has been to map the distribution of molecular gas in the area of L 1521B with a better resolution than has been done so far. This should also provide better estimates for the position and physical parameters of the molecular gas density maximum. Because of its large column density and its location in an active star forming cloud filament the L 1521B core is a promising candidate for being a pre-protostellar core. With this aspect in mind we have also included another area, IRAS 04181+2655 some 1 degree north west of L 1521B in the B216 filament with prominent newly-born stars, into our observing program.

In the L 1521B cloud area several background star positions have been observed for which both optical extinction and polarization values are available; thus our new data provide also a case for studying the correlation between CO column density and optical extinction.

2. Observations

The observations were made during winter 1992-93, spring 1994 and autumn 1995 with the Metsähovi 14-m radiotelescope run by the Helsinki University of Technology. The receiver was a cooled Schottky barrier mixer and the backend a 1728 channel,

Table 2. Fit parameters for the $C^{18}O$(1–0) spectra around IRAS 04181+2655. Column (1) gives the offsets in arc minutes with respect to $04^h18^m06^s$+26°55′00″ (1950.0). The gaussian line parameters are given in columns (2)–(4)

offset (′)	V (km s^{-1})	FWHM (km s^{-1})	T_A^* (K)
(1)	(2)	(3)	(4)
(-1.1, 1.0)	6.41 (0.13)	1.9 (0.3)	1.3 (0.3)
(2.0,-1.0)	6.52 (0.04)	0.85 (0.09)	1.7 (0.2)
(2.0, 1.0)	6.19 (0.04)	0.92 (0.11)	2.1 (0.3)
(2.0, 2.0)	6.03 (0.04)	0.80 (0.08)	2.0 (0.3)
(0.9, 2.0)	6.10 (0.05)	0.92 (0.13)	1.9 (0.3)
(0.0, 2.0)	6.09 (0.04)	0.85 (0.09)	2.2 (0.3)
(-1.1, 2.0)	6.30 (0.05)	1.71 (0.11)	2.1 (0.2)
(-2.0, 2.0)	6.44 (0.07)	1.62 (0.13)	1.3 (0.2)
(-2.0, 1.0)	6.58 (0.04)	1.45 (0.10)	2.1 (0.2)
(-2.0, 0.0)	6.51 (0.06)	0.97 (0.12)	1.6 (0.3)
(-1.1, 0.0)	6.62 (0.03)	1.04 (0.06)	2.7 (0.2)
(0.9, 0.0)	6.61 (0.03)	1.03 (0.07)	2.5 (0.2)
(0.0, 1.0)	6.51 (0.04)	1.53 (0.08)	2.0 (0.2)
(0.0,-1.0)	6.60 (0.03)	0.84 (0.06)	2.5 (0.2)
(0.9, 1.0)	6.33 (0.05)	1.00 (0.13)	2.2 (0.4)
(0.0, 0.0)	6.59 (0.03)	1.18 (0.06)	2.7 (0.2)
(0.9,-1.0)	6.40 (0.05)	1.25 (0.12)	2.3 (0.3)
(-1.1,-1.0)	6.63 (0.03)	0.79 (0.07)	3.6 (0.5)

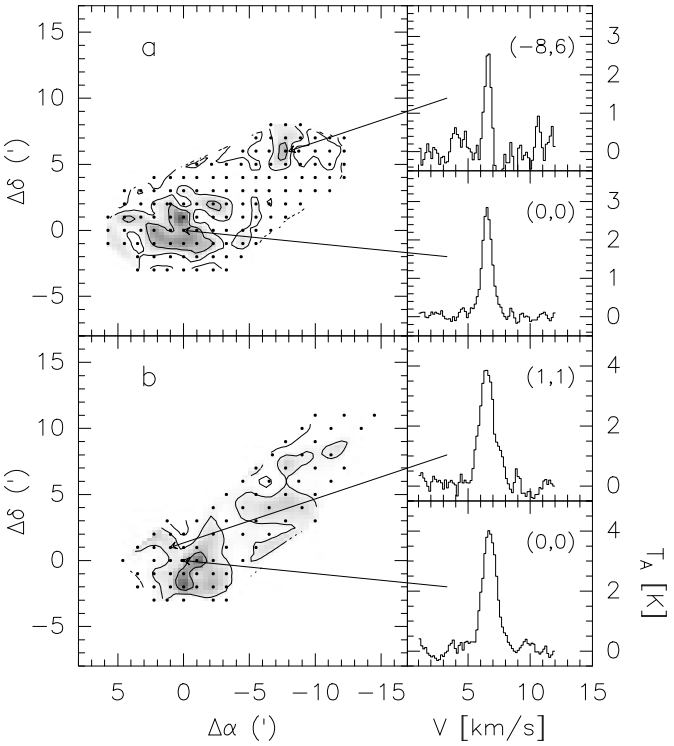

Fig. 2. a The $C^{18}O$(1–0) antenna temperatures in L 1521B. The contours are at 1.2 K, 1.9 K and 2.5 K. **b** The map of the ^{13}CO(1–0) antenna temperatures in L 1521B. The contours are at 3.0 K, 3.6 K and 4.2 K. Examples of spectra are shown at the indicated positions

100 MHz acousto-optical spectrometer with a channel width of 0.16 km s^{-1}. The standard chopper wheel technique was used for calibration. The half power beam width is 1′ for the observed lines.

All observations were made in the frequency switching mode and mostly with a spacing of 1′. In the north-western part of the map the ^{13}CO spectra were measured only at every other point in a chequered pattern. Consistency of the intensity scale was monitored by measurements of Orion A, W3 and by repeated measurements of the centre position of L 1521B. The pointing accuracy is estimated to be better than 15″.

The spectra were first folded and a polynomial baseline of degree 3 to 4 was removed. The observed $T_A^*(C^{18}O)$ for Orion A was scaled to the value given by Ulich & Haas (1976). After this scaling also $T_A^*(C^{18}O)$ at the centre position of L 1521B was identical to the value given by Myers et al. (1983). The ^{13}CO spectra were scaled using the observations of W3 and the value of $T_A^*(^{13}CO)$ given by Ulich & Haas. In L 1521B the scaled value of $T_A^*(^{13}CO)$ agrees within 3% with the value of Myers et al.

3. Results

We present in Figs. 2–4 the results of the mapping of L 1521B. In Fig. 2 we show the distributions of the peak antenna temperatures of $C^{18}O$(1–0) and ^{13}CO(1–0) and in Figs. 3–4 the corresponding maps of integrated intensity. The $C^{18}O$(1–0) spectra measured around IRAS 04181+2655 are shown in Fig. 5.

Because of the relatively high noise levels the spectra were first averaged. New ^{13}CO and $C^{18}O$ spectra were calculated at each position of an observed $C^{18}O$ spectrum. During the averaging process the spectra were weighted with a gaussian with a FWHM of 90″and also according to the noise levels. A single gaussian component was fitted to each averaged spectrum and these results were used in the subsequent calculations. The averaging does not generally change the results obtained from the fits, but makes it possible to make fits also to the weakest spectra with low signal to noise ratios. For selected spectra in L 1521B the fitted line parameters are listed in Table 1 and the parameters of the $C^{18}O$ spectra near the IRAS sources are given in Table 2.

3.1. The derivation of the physical parameters

We derive the optical depth τ_{18} of $C^{18}O$ in the usual manner from the ratio of the measured $C^{18}O$ and ^{13}CO line peak intensities. We assume an optical depth ratio of 5.5 and identical excitation temperatures for both transitions.

The excitation temperature of $C^{18}O$ is calculated as described by Myers et al. (1983). Since the excitation temperature was found to be almost constant the average value of T_{18}=7.3 K was used in the subsequent calculations. The column densities are obtained from the formula:

$$N(C^{18}O) = 2.58 \cdot 10^{14} \mathrm{cm}^{-2} \frac{T_{18}}{1 - e^{-5.2676/T_{18}}} \tau_0 \Delta V, \qquad (1)$$

where τ_0 is the optical depth at the centre of the $C^{18}O$ line and ΔV is FWHM of the $C^{18}O$(1–0) line. In Fig. 6 frames **a** and

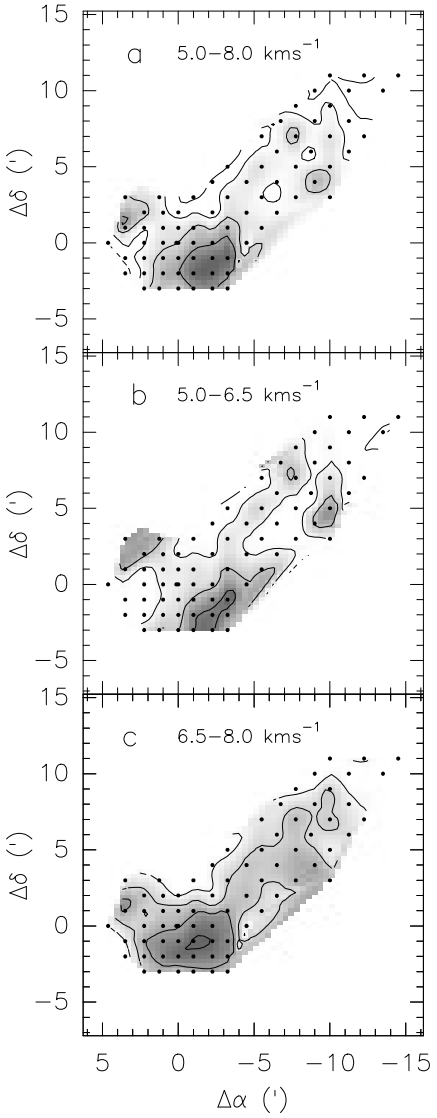

Fig. 3a–c. The map of the integrated ^{13}CO(1–0) emission in L 1521B. **a** Emission integrated over the interval 5.0–8.0 km s^{-1} (the whole line), the contours are at intervals of 0.6 K km s^{-1} starting with 4.5 K km s^{-1}. **b** Interval 5.0–6.5 km s^{-1}, the contours are at intervals of 0.4 K km s^{-1} starting with 1.3 K km s^{-1}. **c** Interval 6.5–8.0 km s^{-1}, the contours are at intervals of 0.4 K km s^{-1} starting with 3.2 K km s^{-1}

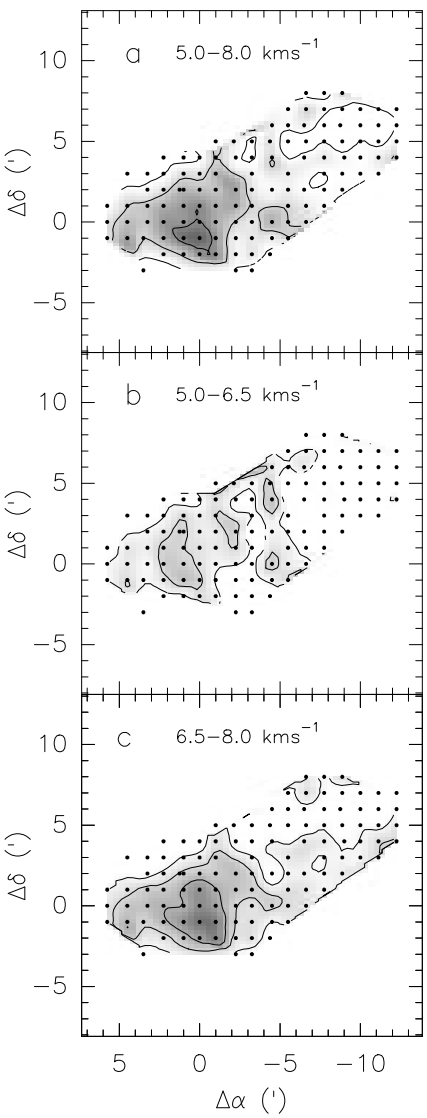

Fig. 4a–c. The maps of the integrated C^{18}O(1–0) emission in L 1521B. **a** Emission integrated over the interval 5.0–8.0 km s^{-1} (the whole line), the contours are at intervals of 0.75 K km s^{-1} from 1.5 K km s^{-1} to 3.0 K km s^{-1}. **b** Interval 5.0–6.5 km s^{-1}, the contours are at 0.6 K km s^{-1} and 0.9 K km s^{-1}. **c** Interval 6.5–8.0 km s^{-1}, the contours are at intervals of 0.35 K km s^{-1} from 1.2 K km s^{-1} to 1.9 K km s^{-1}

b show the distributions of the optical depth and the column density of C^{18}O.

The column density depends strongly on the value of the excitation temperature. If we assume an error of $\pm$2.0 K for T_{18}=7.3 K the errors in the column density N(C^{18}O) induced through Eq. 1 are +51% and -41%. It is unlikely that the excitation temperature could be much lower than the assumed value.

The assumption of identical excitation temperatures for the isotopes ^{13}CO and C^{18}O is also controversial. Due to the high optical depth of the ^{13}CO line it is formed close to the cloud surface, where the gas may be heated by the external UV-field. Therefore, the excitation temperature of ^{13}CO is expected to be somewhat higher than the excitation temperature of C^{18}O which if formed deeper in the cloud. However, the differences in the calculated excitation temperatures of C^{18}O were very small in the mapped region. This indicates that the excitation conditions are not significantly different even between the optically thin regions and the opaque centre. The assumption of a common excitation temperature may therefore be a good approximation.

The column density N(H$_2$) is calculated from N(C^{18}O) as described by Myers et al. (1983):

$$N(\mathrm{H_2}) = 1.7 \cdot 10^{21} + 5.5 \cdot 10^{6}\ N(\mathrm{C^{18}O}) \qquad (2)$$

This is a result of the relation between N(H$_2$) and A_V given by Bohlin et al. (1978) and the relation between A_V and N(C^{18}O) given by Frerking, Langer and Wilson (1982) (see

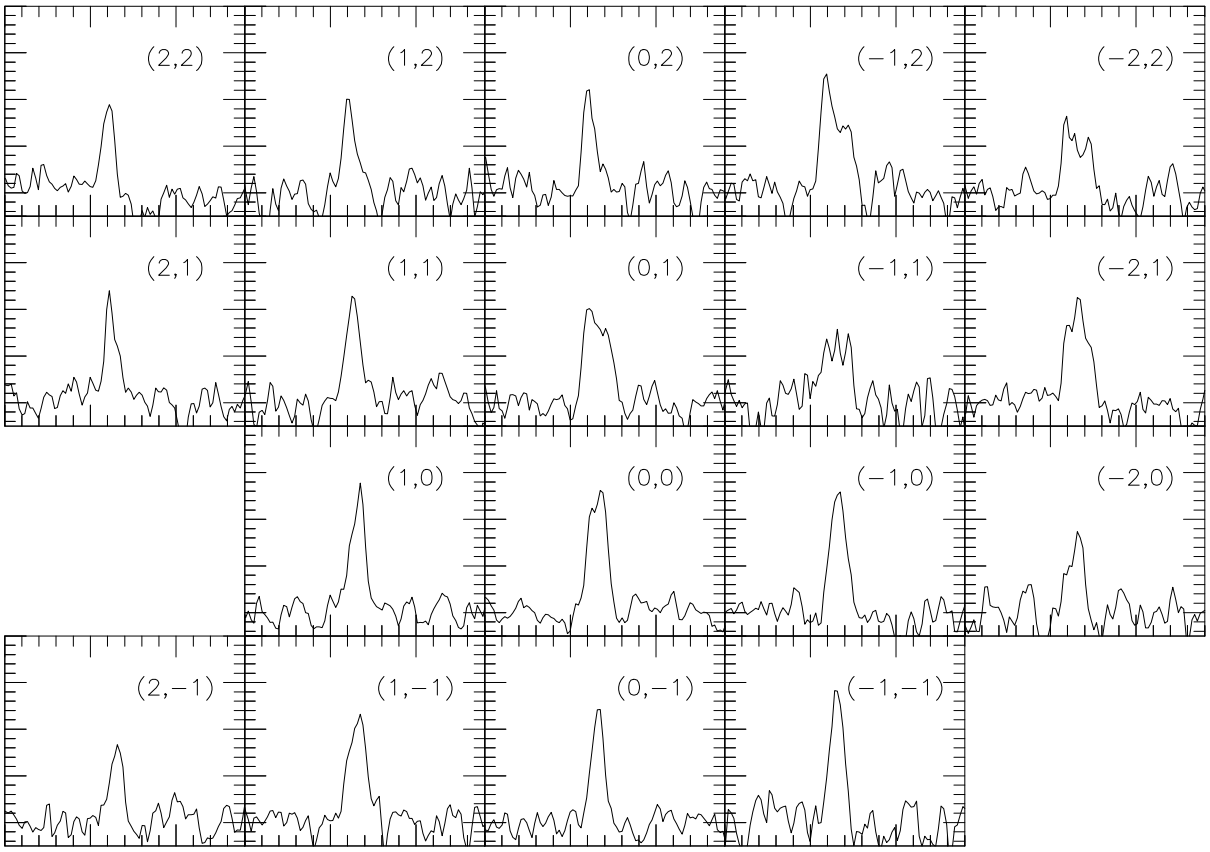

Fig. 5. The observed $C^{18}O$(1–0) spectra around the IR source 04181+2655. The centre position is $4^h18^m6^s.0+26°55'00''$ (1950.0) and the offsets are shown arc minutes. The plotted velocity range is 0.0–14.0 km s^{-1} and the T_A^*–range is from -0.5 K to 4.0 K. The dashed lines indicate the velocity of 6.5 kms^{-1}

Myers et al. 1983). For the central point of L 1521B we get $N(C^{18}O)=4.2\cdot10^{15}$ cm^{-2} and $N(H_2)=2.5\cdot10^{22}$ cm^{-2}.

Dividing the maximum column density $N(H_2)$ = $2.5\cdot10^{22}$ cm^{-2} with 0.33 pc corresponding to 8′ gives an average density of $2.5\cdot10^4$ cm^{-3} for the whole core.

The density in the centre of L 1521B was estimated by assuming a spherically symmetric density distribution and by using the derived H_2 column density values to estimate the radial density structure. This procedure gives a central density of $n(H_2)=2.8\cdot10^4$ cm^{-3}. Only the observations within a 6′ wide band running across the centre at right angles with the axis of the filament were used. Since the column density at the edges of this area is still about one third of the central value this density should be an upper limit. On the other hand, since the actual density distribution is not spherical but elongated the fitted density distribution is also flatter than the real one.

The column densities $N(H_2)$ were used to calculate also the mass distribution over the mapped area. The mass contained within a radius of 3′ from the centre of the cloud is found to be about 20 solar masses. The column density has its the maximum close to the centre position. There the column density gives a mass of about 0.8 solar masses per square arc minute, i.e., a pixel of 0.04 × 0.04 pc^2. These values are consistent with the results of Myers et al. (1983) and Gaida et al. (1984).

The mass is not distributed symmetrically, however, and there is no clear separation between the cloud core and the extended less dense filament. Much of the mass in the mapped region is beyond the radius of 3′. In the column density map the contours denoting half of the maximum value extend beyond the map in the south-east direction along the filament. The estimated mass within the whole map area (some 110 square arc minutes) amounts to about 59 $M_\odot$.

3.2. Correlation $C^{18}O/A_V$

Within or very near the mapped area there are six background stars for which the colour excesses E_{J-K} are known (Goodman et al. 1992). These are given in Table 3 which also contains the values of the visual extinction calculated from $A_V = 5.3\,E_{J-K}$ (see Harjunpää & Mattila 1996). In Fig. 7 we present the column densities of $C^{18}O$ as a function of A_V. Three of the stars are within the mapped area and are marked with solid squares in the figure. The other three stars are outside the the mapped area but no further than 1.5′ from an observed position. The column densities at these positions are uncertain and they are marked with crosses in the figure.

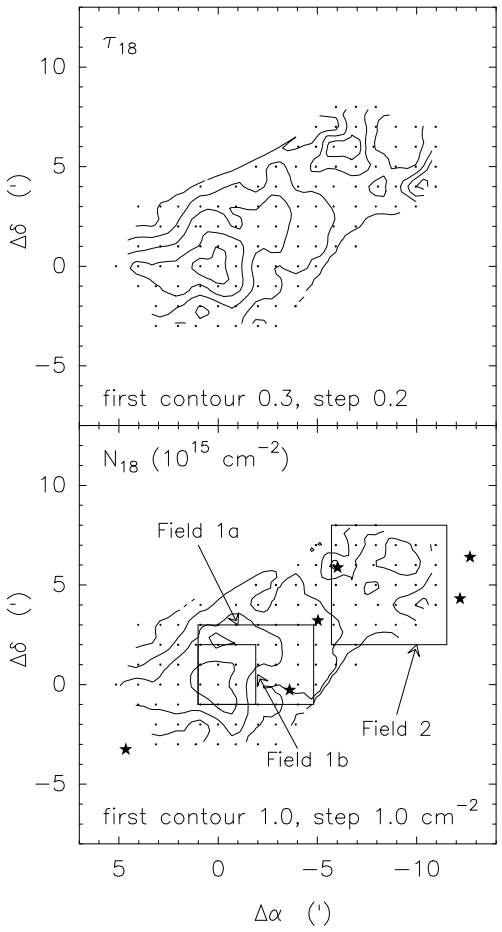

Fig. 6a,b. Maps of the physical quantities derived from the observations of L 1521B. The coordinate offsets are with respect to the centre position of L 1521B, $4^h21^m8.5^s$+26°30′00″ (1950.0). **a** The optical depth of the $C^{18}O$ line. **b** The column density of $C^{18}O$. The asterisks indicate the background stars observed by Goodman et al. (1992). The fields observed in near infrared and used for star counting in this article are also marked in the figure

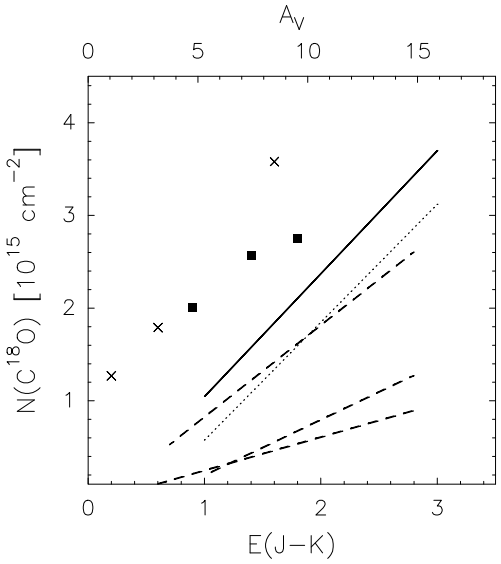

Fig. 7. The relation between E_{J-K} and the $C^{18}O$ column density. The filled squares indicate the background stars within the area mapped in $C^{18}O$ and the crosses represent stars near the map borders. The solid line denotes the relation given by Duvert et al. (1986) based on observations of L1495 and the dotted line the fit of Frerking et al. (1982) for Taurus clouds with $A_V > 5^m$. The three dashed lines show the relation for Cha I (the upper line), R CrA (in the middle) and Coalsack (the lower line) (Harjunpää & Mattila 1996)

In Fig. 7 we also show the least squares line of Duvert et al. (1986) derived from the observations of the cloud L1495 which is located at the north-west end of the filament containing L 1521B. This is very similar to the result of Frerking et al. (1982) (shown as a dotted line), $N(C^{18}O)=2.4\cdot10^{14}\,(A_V-2.9)\,cm^{-2}$, which applies to clouds in Taurus with $A_V > 5^m$. Our observations are in general agreement with these relationships. We have also included for reference the lines for Cha I, R CrA and Coalsack given by Harjunpää & Mattila (1996). Due to differences in the derivation of the column densities the $N(C^{18}O)$ values of the references may not be directly comparable.

We fitted a line to our observations with the slope fixed to the average value of the relation given by Frerking et al. and the relation given by Harjunpää & Mattila for Coalsack. Such a slope is also consistent with our data. For the stars at the edge of the mapped region the errors in $N(C^{18}O)$ were taken to be twice as high as the errors for the stars inside the map. Using this line we derived a value for the visual extinction at the centre of L 1521B. Using a column density value of $N(C^{18}O)=4.2\cdot10^{15}\,cm^{-2}$ we get first $E_{J-K}=3.5$ and, by multiplying this with 5.3, $A_V=18.6^m$. The relation of Bohlin et al. (1978), $N(H_2)=0.94\cdot10^{21}\,A_V$, gives $N(H_2)=1.7\cdot10^{22}\,cm^{-2}$, which is somewhat lower than the value calculated earlier from the relation of A_V vs. $N(C^{18}O)$ used by Myers et al. (1983).

The extinction in L 1521B has also been determined using star count data at 2.2 μm (K) obtained with the near-IR camera (MAGIC) at the 2.2 meter telescope of the Calar Alto Observatory. The NICMOS3-type array has 256×256 pixels and was used in the wide field mode with 1.6 arc sec/pixel, corresponding to a 6.8×6.8 arc min field size. The frames were calibrated and reduced to outside the atmosphere using standard stars. For the 500 sec exposure time the limiting magnitude was ~ 16.

Two fields were observed in the obscured area of L 1521B. Their positions are indicated in Fig. 6b. For the eastern field two subfields are indicated, field 1a and 1b. Two comparison areas (OFF positions) were observed in the relatively transparent area south of L 1521B. They were located 11′ south of each of the dark cloud (ON) positions. To determine the K band extinction we used the Wolf method as applied e.g. by Bok (1956), i.e. only the cumulative star counts, N(m), to the (uniform) limiting magnitude, m, of the data set are used. In addition, the slope of the log N(m) vs. m curve is needed. Its value was obtained from the recent K band star counts of Beichman and Jarrett (1994) covering a 3 □° area in Taurus, some 4°east of L 1521B. Its value is 0.32.

Table 3. The background stars in the L 1521B region. The stars located near the borders of the mapped region are marked with a dagger. In the column (3) are the the values of E_{J-K}=(J–K)-1.0 from the article by Goodman et al. (1992). The values in column (4) have been calculated from A_V=5.3 E_{J-K} and the column (5) gives the column densities of $C^{18}O$ derived from our observations

α (1950)	δ (1950)	E_{J-K}	A_V	N($C^{18}O$) [10^{15} cm^{-2}]	
(1)	(2)	(3)	(4)	(5)	
4 20 11.7	26 36 24	0.6	3.18	1.8	†
4 20 14.0	26 34 19	1.6	8.48	3.6	†
4 20 41.6	26 35 53	1.8	9.54	2.8	
4 20 46.0	26 33 13	1.4	7.42	2.6	
4 20 52.4	26 29 44	0.9	4.77	2.0	
4 21 29.3	26 26 45	0.2	1.06	1.3	†

We give in Table 4 the results of the star counts in L 1521B. The average number of stars counted in the two reference fields corresponds to 7580±600 stars with K≤16 per □°. This is in excellent agreement with the star counts of Beichman and Jarrett (1994) which, when extrapolated from their limiting magnitude of 14.5 to 16.0, give the result N(K $\leq$ 16) $\approx$ 7100 stars per □°. The cloud extinction is given with respect to an assumed zero extinction level for the reference fields. The small field 1b corresponds approximately to the maximum extinction and CO column density area in L 1521B. We obtain for it the minimum extinction of $A_V \gtrsim 25^m$ corresponding to the estimated upper limit of 4 stars in the counted area of 8.7 □′. Taking the actually counted number of 2 stars in this field gives an extinction of $A_V \approx 33^m$. In the larger field 1a where we have better counting statistics (total number of stars is 8) we obtain the extinction A_V = 20^m. The extinction estimate obtained from the $C^{18}O$ column density is thus in good general agreement with the star count result.

3.3. Discussion

The antenna temperature maps (Fig. 2) are rather similar in for both isotopes. The emission peaks are in both lines approximately at the the adopted centre position, $04^h21^m08.6^s$+26°30′00″(1950.0). The emission region is slightly elongated along the filament, as expected, but in the centre the contour lines are almost circular. The ^{13}CO emission is strong over the whole map. The peak value of 4.9 K is measured at a point adjacent to the centre position, but even at the outermost points towards north-west the antenna temperatures are still around 3.0 K. Strong ^{13}CO emission clearly extends along the filament far beyond the mapped region. This can, of course, be seen also from the maps by Fukui and Mizano (1992). The $T_A^*(C^{18}O)$ maximum is 3.1 K at the centre of L 1521B.

The maximum of the integrated ^{13}CO emission (Fig. 3) is clearly displaced towards south-west compared with the map of peak antenna temperatures (Fig. 2) or the map of the integrated $C^{18}O$ emission (Fig. 4). This is apparently the result of changes in the ^{13}CO linewidths.

The maps of integrated ^{13}CO emission indicate also some changes in the line velocities over the central region. At smaller velocities the emission maximum is more clearly displaced towards south-west. The velocity gradient seems therefore to be perpendicular to the filament and directed towards north-east. The change is almost unnoticeable in the parameters of the fitted gaussians, however. Closer inspection of the spectra shows, that the feature may be due to a change in the line profiles. The centre spectrum and the spectra immediately to the east and to the north of the centre position have some redshifted wing emission (see Fig. 2b). The wing can be clearly seen in altogether six spectra and it is therefore unlikely to be an artifact caused by the noise. Due to this feature the maximum of the ^{13}CO emission integrated from 6.5 kms^{-1} to 8.0 kms^{-1} is close to the map centre. Myers et al. (1983) also noted that their ^{13}CO(1–0) spectrum at the centre of L 1521B was skewed to lower velocities.

In the maps of integrated $C^{18}O$ emission one cannot see similar velocity shift as in the ^{13}CO maps. Therefore, the maps of the two isotopes are very similar at higher velocities while at lower velocities the ^{13}CO maximum is shifted several arc minutes from the $C^{18}O$ maximum.

There are many possible explanations for this difference. Most likely it is simply due to different distributions of the dense and the more diffuse gas, with the diffuse gas being more concentrated to the south-western part of the area. In that case the red wing seen in the ^{13}CO spectra north-east of the centre position might actually have a more symmetric distribution relative to the cloud centre. The fact that it is not distinctly seen towards south-western part of the centre could be due to blending or shielding by the diffuse gas the velocity range of which covers also the red wing.

The red wing emission could be interpreted as a sign of systematic motions, e.g. contraction in the central regions of L 1521B. The wing emission might, however, originate also from some smaller clump with a radial velocity that is a little higher than the radial velocity of the rest of the gas seen in ^{13}CO.

The radial velocity is remarkably constant along the filament in spite of the large scale velocity gradient directed towards south-east (see e.g Heyer 1987). Taking the parameters of the gaussians fitted to the six ^{13}CO spectra furthest towards north we obtain an average radial velocity of 6.59±0.05 km s^{-1}, while the average velocity of the 3×3 spectra around the centre position is 6.64±0.05 km s^{-1}. Thus the gradient is almost non-existent within the mapped area. Since the gaussian fits near the centre might also be affected by the existence of the redshifted wing emission, one can conclude that no systematic velocity gradient can be seen along the filament at this scale. This is confirmed by the fact that the average radial velocity of the points at the bottom row of the map is 6.61±0.04 km s^{-1}.

The changes in the linewidths of ^{13}CO(1–0) are more pronounced. Taking again the results of the gaussian fits to the six spectra in the north-western corner of the map one gets an average linewidth of 1.29±0.09 km s^{-1}. This is the area with the narrowest line profiles. As one approaches the core centre along the filament, the mean linewidth rises only slightly. The average for the nine spectra at the centre of L 1521B is 1.47±0.12 km s^{-1}. The increase in the linewidths is stronger south-west of the cloud centre, and the average for the 3×3 spectra in the lower

Table 4. Extinction estimates from K band star counts in L 1521B. The table contains the number of stars observed in each field, the field area, cumulative star count number per $\square^\circ$, the estimated K band extinction and the visual extinction. The values in parentheses give the 1σ estimates for errors caused by the star counting statistics

	Field 1a	Field 1b	Field 2	Ref. 1	Ref.2
No. of stars ($K \leq 16^m$)	8	2 ± 2	37	75	72
Area ($\square'$)	21.8	8.7	34.9	34.9	34.9
N(m) per sq. degree	1300(500)	400(400)	3800(600)	7700(900)	7400(800)
A_K	2.4 (0.5)	≥ 3.0	0.9(0.2)		
$A_V = A_K/0.12$	20 (4)	≥ 25	7.5(1.7)		

right hand corner of the map is already $1.78 \pm 0.10\,\mathrm{km\,s^{-1}}$. This explains the displacement of the emission maximum towards south-west as seen in the maps of integrated antenna temperatures in Fig. 3. Although a similar trend seems to exist also north-east of the centre this is less pronounced. However, the two spectra furthest to this direction from the centre position have line widths of over $1.7\,\mathrm{km\,s^{-1}}$.

The $C^{18}O$(1–0) line has a linewidth of $1.03\,\mathrm{km\,s^{-1}}$ and a velocity of $6.55\,\mathrm{km\,s^{-1}}$ at the centre position of L 1521B. The $C^{18}O$ emission around the IRAS point sources situated about one degree north-west of L 1521B is only slightly less intense than in L 1521B. The emission is also nearly constant within the small region that was mapped and beam dilution should not be a problem. The narrowest lines have linewidths comparable to those in L 1521B i.e. about $0.9\,\mathrm{km\,s^{-1}}$. At the position (0,-1) in Fig. 5 i.e. at the location of the IR source 04181+2654 the linewidth is even less i.e. $0.84\,\mathrm{km\,s^{-1}}$. At the position of the IR source 04181+2655 (0,0) the fitted gaussian has a centre velocity of $6.59\,\mathrm{km\,s^{-1}}$ and a width of $1.18\,\mathrm{km\,s^{-1}}$. Considering the noise level the spectrum cannot be said to be significantly broader than the rest of the narrower spectra. Moriarty-Schieven et al. (1992) have observed CO(3–2) at this position. They detected a possible blue wing in the CO(3–2). The spectra north and north-west of the IRAS sources have, however, much more clearly non-gaussian profiles. At the position (0,1) the line is already much broader (Δv =1.53 $\mathrm{km\,s^{-1}}$) and may also display some self-absorption. All spectra towards north and north-west of the centre are significantly broader than the spectrum at the position (0,0) and have non-gaussian profiles. There is also a clear change in the radial velocities. The profiles between (1,-1) and (1,2) might even lead one to suspect the existence of two velocity components. The lines east of these show, however, only one emission component with a velocity gradient. The gradient points approximately to south-west with the radial velocity changing from about $6.1\,\mathrm{km\,s^{-1}}$ at the upper left hand corner of the map to $6.6\,\mathrm{km\,s^{-1}}$ at the position (-1,-1).

With the advent of sensitive wide angle array -cameras the near–IR star counts provide a powerful new technique for the determination of interstellar extinction. It is of special importance in the case of dense cores which are too opaque to be studied by optical star counts or photometry. Lada et al. (1994) have presented an extensive near–IR extinction study of the dark cloud IC 5146. Their method combines both color index and star count information in the JHK bands, with a limiting magnitude of m_K=13.1^m. Our results for L 1521B demonstrate that even star counts in a single filter-band alone can provide a good estimate for the extinction. In order to have sufficient count statistics for a small core area like L 1521B the limiting magnitude should be $m_K \approx 16^m$ as in our case or fainter. Such limiting magnitudes can be routinely reached with the state-of-the art near–IR array cameras at medium-size telescopes. In the near future the DENIS and 2MASS surveys will start providing near-IR star count data over the whole sky (cf. Epchtein et al. 1994, Kleinmann et al. 1994). One obvious application will be the detection and extinction determination of very opaque molecular cloud cores.

4. Conclusions

We have mapped in B216 the dark core L 1521B in ^{13}CO(1–0) and in $C^{18}O$(1–0). The area in B213 containing the IRAS sources 04181+2655 and 04181+2654 has been mapped in $C^{18}O$(1–0). These two areas are situated in the same filamentary structure and within a distance of about one degree. The IR sources are probably associated with class I protostars while no star formation activity has been detected in L 1521B so far.

The observations have shown that

1. L 1521B is a local density enhancement of the filament and cannot be clearly separated from the large scale structure
2. The $C^{18}O$ column density has a maximum of $4.2 \cdot 10^{15}\,\mathrm{cm^{-2}}$ in L 1521B and the mass contained within a radius of 3′ is some $20\,M_\odot$; the central density is estimated to be about $n(H_2)=2.8 \cdot 10^4\,\mathrm{cm^{-3}}$
3. The relation between $N(C^{18}O)$ and A_V is found to be similar to that previously found in other regions in Taurus
4. Using this relation between $N(C^{18}O)$ and A_V we estimate that at the centre position of L 1521B A_V=18.6^m and $N(H_2)=1.7 \cdot 10^{22}\,\mathrm{cm^{-2}}$; star counts give an extinction of $A_V \approx 20^m$ for the central region and indicate a peak value $A_V \gtrsim 25^m$
5. The $C^{18}O$ line widths are not significantly different in the quiescent core L 1521B and the location of IRAS 04181+2655 known to be associated with young protostars
6. The $C^{18}O$(1–0) spectra around IRAS 04181+2655 show a strong velocity gradient and non-gaussian line profiles
7. We have not found evidence for a protostellar condensation in L 1521B: however, weak red wing emission in the ^{13}CO(1–0) spectra near the centre of L 1521B is present and

may be indicative of systematic motions related to an early protostellar phase in the core evolution

References

Barnard, E.E. 1927, Atlas of selected regions in the Milky Way, eds. E.B. Frost, M.M. Calvert, Carnegie Institute of Washington

Beichman, C.A., Jarrett, T. 1994, Ap&SS 217, 207

Benson, P.J., Myers, P.C. 1989, ApJS 71, 89

Bohlin, R.C., Savage, B.D., Drake, J.F. 1978, ApJ 224, 132

Bok. B.J. 1956, AJ 61, 309

Cernicharo, J., Bachiller, R., Duvert, G. 1985, A&A 149, 273

Cernicharo, J., Bachiller, R., Duvert, G. 1986, A&A 160, 181

Cox, P., Walmsley, C.M., Güsten, R. 1989, A&A 209, 382

Crutcher, R.M., Troland, T.H., Goodman, A.A. et al. 1993, ApJ 407, 175

Duvert, G., Cernicharo, J., Baudry, A. 1986, A&A 164, 349

Frerking, M.A., Langer, W.D., Wilson, R.W. 1982, ApJ 262, 590

Epchtein, N., DeBatz, B., Copet, E. et al. 1994, Ap&SS 217, 3

Fukui, Y., Mizuno, A. 1991, A Comparative study of Star Formation Efficiencies in Nearby Molecular Cloud Complexes, in Falgarone, E., Boulanger, F., Duvert, G. (eds) IAU Symposium 147, Fragmentation of Molecular Clouds and Star Formation. Kluwer, Dordrecht, p. 275

Gaida, M., Ungerechts, H., Winnewisser, G. 1984, A&A 137, 17

Goodman, A., Jones, T., Lada, E., Myers, P. 1992, ApJ 399, 108

Harjunpää, P., Mattila, K., 1996, A&A 305, 920

Heyer, M.H., Vrba, F.J., Snell, R.L. et al. 1987, ApJ 321, 855

Kenyon, S., Hartmann, L., Strom, K., Strom S. 1990, AJ 99, 869

Kenyon, S., Calvet, N., Hartmann, L. 1993, ApJ 414, 676

Kleiner, S., Dickman, R. 1984, ApJ 286, 255

Kleinmann, S.G., Lysaght, M.G., Pughe, W.L. et al. 1994, Ap&SS 217, 11

Lada, C.J, Lada, E.A., Clemens, D.P., Bally, J. 1994, ApJ 429, 694

Moneti, A., Pipher, J., Helfer, H., McMillian, R., Perry, M. 1984, ApJ 282, 508

Moriarty-Schieven, G.H., Wannier, P.G., Tamura, M., Keene, J. 1992, ApJ 400, 260

Myers, P.C., Fuller, G.A., Goodman, A.A., Benson, P.J 1991, ApJ 376, 561

Myers, P.C., Ho, P.T.P., Benson, P.J. 1979, ApJ 233, L141

Myers, P.C., Linke, R.A., Benson, P.J. 1983, ApJ 264 517

Sorochenko, R.L., Tolmachev, A.M., Winnewisser, G. 1986, A&A 155, 237

Tamura, M, Sato, S., 1989, AJ 98, 1368

Tamura, M., Gatley, I., Waller, W., Werner, M.W. 1991, ApJ 374, L25

Terebey, S., Shu, F.H., Cassen, P. 1984, ApJ 286, 529

Ulich, B.L., Haas, R.W. 1976, ApJS 30, 247

Ungerechts, H., Thaddeus, P. 1987, ApJS 63, 645

This article was processed by the author using Springer-Verlag LaTeX A&A style file *L-AA* version 3.